Applied Acoustics 73 (2012) 379–385

Contents lists available at SciVerse ScienceDirect

Applied Acoustics

journal homepage: www.elsevier.com/locate/apacoust

MEMS electrodynamic loudspeakers for mobile phones

G. Lemarquand [a,*], R. Ravaud [a], I. Shahosseini [c], V. Lemarquand [b], J. Moulin [c], E. Lefeuvre [c]

[a] Universite du Maine, LAUM, UMR CNRS 6613, Le Mans, France
[b] Universite de Toulouse, LAPLACE, UMR CNRS 5213, IUT Figeac, France
[c] Universite Paris Sud, IEF, UMR CNRS 8622, France

ARTICLE INFO

Article history:
Received 18 March 2011
Received in revised form 26 October 2011
Accepted 28 October 2011
Available online 25 November 2011

Keywords:
MEMS
Loudspeaker
Acoustic transducer
Voice coil motor

ABSTRACT

This paper presents a MEMS structure of electrodynamic loudspeakers dedicated to mobile phone applications. The major goals are to obtain a high electroacoustic conversion efficiency and a high fidelity acoustic quality. The originalities lie in a rigid silicon membrane and in its suspension by a set of silicon beams. The moving coil is a planar copper microcoil electroplated on the silicon membrane whose microstructure was optimized for providing both rigidity and lightness of the mobile part.

This paper presents different magnetic structures of the motor for this MEMS loudspeaker. These structures are ironless, only made out of permanent magnets which are bonded on the substrate. They are studied and optimized thanks to analytical formulations of the magnetic field created by the permanent magnets. Results are presented for a deep RIE etched 7.5 mm radius silicon membrane structured with 40 stiffening ribs and on a 30 μm thick microcoil with 35 turns.

1. Introduction

Microspeakers with high power and good acoustic quality are increasingly required by the mobile device users. These users and consumers represent a quickly growing part of the society and the youngest among them require a mobile acoustic source which allows the music listening in good conditions. Moreover, the autonomy of mobile devices is a critical issue. Reducing their consumption is strategic. For instance, up to one quarter of the total energy is consumed by the audio system in cellular phones in free hand mode. Furthermore, microspeakers used in mobile devices have a very poor sound quality compared to that of conventional loudspeakers. As a consequence, a new loudspeaker was designed to address these drawbacks.

The acoustical quality is directly related to the mobile face vibration modes. Ideally, these modes should not appear in the loudspeaker bandwidth. They are a function of the material Young's modulus, E, over its volume density, ρ. With a value of $\frac{E}{\rho} = 71$ (MPa m^3/kg), the silicon is one of the best materials. This ratio value increases threefold with regard to the one obtained for aluminum or titanium.

The monocrystaline silicon is not sensitive to mechanical fatigue, so this material can also be used for the membrane suspension beams. This is already used in the design of MEMS accelerometers, but the displacements for the loudspeaker are far greater.

Besides, the motor is a voice-coil one with a planar copper coil electroplated on the silicon membrane. The magnetic circuit is ironless and only constituted of permanent magnet rings which are bonded to the silicon substrate. The device is designed and optimized to reach the intended performances. Therefore, several motor structures are presented and compared.

It has to be noted that such a MEMS is a very novel device which presents improvements at several levels. This loudspeaker is electrodynamic but its ironless motor [1] suppresses the non-linearity source constituted by the iron in classical structures and gives the device a very linear behavior, with extremely low distortion. Moreover, its force factor is quite high and its inductance is both low and constant. These are consequent improvements with regard to classical electrodynamic motors. Furthermore, the moving part being very light leads to an increased efficiency. Moreover, the silicon emissive surface is plane and perfectly rigid. As a consequence, it works as a piston and the first surface deformation mode is a drum one at a frequency rather high in the bandwidth, which is really noteworthy. As for the MEMS point of view, these devices are generally used for small dimensions and small movements of a few micrometers. But the present device is designed for displacements in the range of 600 μm peak to peak, which is really a huge range with regard to typical values. So, to our knowledge, the presented device is the first MEMS electrodynamic loudspeaker and it combines advances in electrodynamic loudspeakers as well as in the MEMS technology.

* Corresponding author. Address: LAUM, Avenue Olivier Messiaen, 72085 Le Mans Cedex 9, France.
E-mail address: guy.lemarquand@ieee.org (G. Lemarquand).

0003-682X/$ - see front matter © 2011 Elsevier Ltd. All rights reserved.
doi:10.1016/j.apacoust.2011.10.013

2. Description

As shown in Fig. 1, a planar coil is located on top of the membrane. The copper track is rather thick and needs a specialist technique to be deposited [2]. Its electrical supply is achieved via two conductive tracks which are supported by the suspension beams. Moreover, the coil is protected from short circuits by an electrically insulating layer with two vias which is located between the coil and the conductor tracks. These elements and the membrane define the microspeaker mobile part. Furthermore, two magnet rings are located on each side of the substrate and are completely surrounding the coil to induce a maximal radial magnetic field. Besides, this figure also shows an inset of microstructures on the membrane backside, which is studied in the next part.

3. Moving part

Instead of the deformable diaphragms used in most of the MEMS microspeakers to generate acoustic waves [3–7], a stiff and light membrane is employed here. Usually, the diaphragm, made in a material such as parylene or polyimide, is clamped to the substrate on its external edge. Consequently, the principal vibration mode of such microspeakers is the drum mode. However, with the use of a rigid membrane held by low stiffness suspension beams the fundamental vibration mode is the piston mode: the whole surface of the membrane always runs parallely to its original position.

The modal analysis with FEM modeling of a non-structured membrane reveals that at least 20 proper modes occur in the frequency bandwidth. This phenomenon deteriorates the sound quality. This problem is overcome by the microstructuration of the back side of the membrane as described in [8]. Indeed, while that membrane becomes thicker, so more rigid, holes dug in the membrane make it lighter. Consequently the vibration modes will shift to higher frequencies. In this way, a ribbed structure was designed as depicted in Fig. 2. Each structural element – rib thickness and width, central circle radius, rib number – is optimized on the basis of a trade-off between the vibration mode shift and the membrane total weight. A careful analysis proves that for a membrane with 40 ribs and a 83% weight reduction only five undesired vibration modes appear in the bandwidth.

4. Copper microcoil

We tried to design a coil whose weight approximately equals the membrane one and whose position is as peripheral as possible on the membrane in order to be located in the region of intense magnetic field. This microcoil must be very thick: 35 turns 30 μm thick were wound between the 5 mm inner radius and the 7.5 mm outer one (Fig. 3) and its microfabrication steps were carefully optimized [8]. Its measured resistance is 12 Ω and its inductance 10 μH.

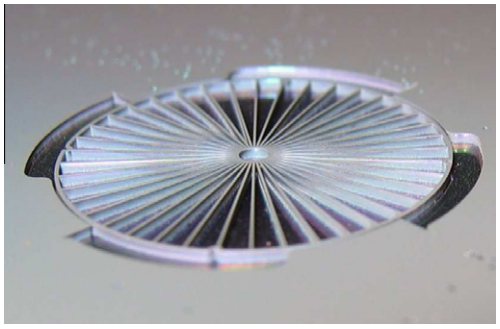

Fig. 2. Membrane back side: photograph of a prototype.

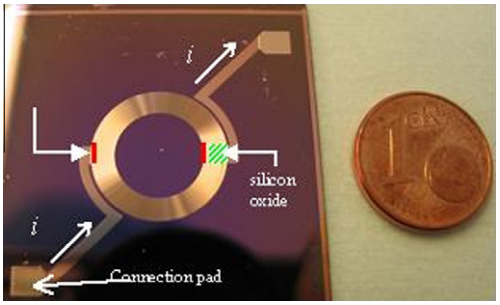

Fig. 3. Micro-coil general top view: prototype photograph, the size is given by the 1 euro cent coin.

5. Acoustic performances

5.1. Electrodynamic loudspeaker equations

The electrical and mechanical equations describing the electrodynamic loudspeaker are the following:

$$U = R_e i + L_e di/dt + Blv \quad (1)$$

$$M_{ms}\gamma = Bli - x/C_{ms} - R_{ms}v \quad (2)$$

where U and i are the voltage and the current, R_e and L_e the electrical resistance and inductance, B is the average radial magnetic induction, l the moving coil length, Bl the force factor, x, v and γ are the position, speed and acceleration of the moving part, M_{ms} is the moving part mass, C_{ms} and R_{ms} the compliance and the damping coefficient of the suspensions. These equations are easily solved in the sinusoidal mode and lead to the expression of Eq. (3) for the speed:

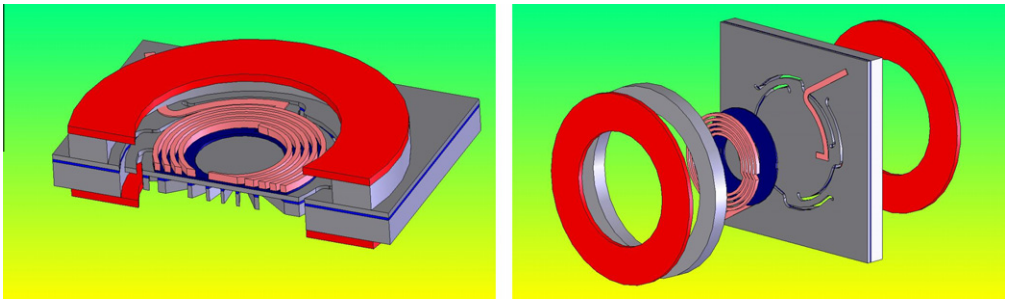

Fig. 1. Cross-section view and exploded view drawn with a CAD tool. Layer materials: neodymium iron boron magnet (red), silicon (gray), copper (pink), silicon oxide (blue). Moving membrane radius: 7.5 mm, membrane minimum thickness: 20 μm, copper coil thickness: 30 μm.

$$v = \frac{Bli}{R_{ms} + j\omega M_{ms} + \frac{1}{j\omega C_{ms}}} \quad (3)$$

5.2. Loudspeaker bandwidth

Because of its shape the emissive face has the behavior of a plane piston [9,10]. So, it creates a simple, spherical and non-directional wave as long as:

$$kr < 1 \quad (4)$$

where k is the wave number and r the moving face radius. This defines the upper limit of the frequency bandwidth, f_u:

$$f_u = \frac{c}{2\pi r} \quad (5)$$

where c is the sound celerity. The dispersion mechanical impedance, Z_{mr}, is defined as follows:

$$Z_{mr} = R_{mr} + X_{mr} = F/v \quad (6)$$

where F is the exerted force and v the membrane speed. For the frequencies lower than f_u, the real part of this impedance is:

$$R_{mr} = \frac{\rho_{air}}{c}\frac{\pi}{2}\omega^2 r^4 \quad (7)$$

where ρ_{air} is the air density. The acoustic power radiated by the front face of this circular plane is the following:

$$W_{ac} = R_{mr} v^2 \quad (8)$$

Eqs. (7) and (8) lead to:

$$W_{ac} = \frac{\rho_{air}}{c}\frac{\pi}{2} r^4 \gamma^2 = 5.510^{-3} r^4 \gamma^2 \quad (9)$$

So, the acoustic power is proportional to the square of the moving part surface area and acceleration. Moreover, for a given acoustic power, the acceleration is also given. Consequently, the membrane maximal displacement, x_{max} sets the lower limit of the frequency bandwidth, f_l and

$$f_l = \frac{1}{2\pi}\sqrt{\frac{\gamma}{x_{max}}} \quad (10)$$

Eq. (10) shows that the lowest working frequency defines the membrane peak displacement for a given radius. As the new standard for high fidelity mobile audio systems stands, the target has been set to 70 dB SPL at 10 cm, and the bandwidth from 300 Hz to 20 kHz. Indeed, these are the requirements of both the smart phone manufacturers and the mobile phone network operators, although no new norm has been edited by now. The thickness and displacement limits defined for this microspeaker have led to a 7.5 mm radius for the membrane. Then, the acoustic dispersion is perfectly non-directional up to a 7 kHz frequency. Furthermore, for such a size of the emissive face the 70 dB SPL at 10 cm acoustic level is reached if the acceleration equals 740 m/s^2 (root mean square value) over the whole frequency bandwidth. Moreover, the membrane displacement range is determined by the lowest frequency for which this acoustic level, so this acceleration, must be reached. A 600 μm peak to peak displacement corresponds to a low frequency equal to 300 Hz, so a −3 dB cutoff frequency equal to 250 Hz.

5.3. Efficiency

The loudspeaker is a system with a resonance frequency, f_r, which is defined by:

$$2\pi f_r = \sqrt{\frac{1}{M_{ms} C_{ms}}} \quad (11)$$

For frequencies higher than the resonance frequency, $f \gg f_r$, the velocity defined in Eq. (3) becomes:

$$v = \frac{Bli}{j\omega M_{ms}} \quad (12)$$

Then for a frequency in the loudspeaker bandwith, $f_r \ll f \ll f_u$, the acoustic power (Eqs. (8) and (7)) is:

$$W_{ac} = \frac{\rho_{air}}{c}\cdot\frac{\pi}{2}\cdot\frac{(Bl)^2\cdot r^4}{M_{ms}^2}\cdot i^2 \quad (13)$$

So, the acoustic power varies as the square of the current in the coil. For small loudspeakers as the considered ones the acoustic power, W_{ac}, is far smaller than the consumed electric power, W_{elec}:

$$W_{elec} = W_{ac} + R_e i^2 \simeq R_e i^2 \quad (14)$$

Moreover, the electric resistance of the moving coil, R_e, is expressed as a function of its mass, M_{cop}:

$$R_e = \rho^*_{cop}\rho_{cop}\frac{l^2}{M_{cop}} \quad (15)$$

where ρ^*_{cop} is the copper density and ρ_{cop} its resistivity. Then, the efficiency of the device is:

$$\eta = \frac{W_{ac}}{W_{elec}} = \frac{W_{ac}}{R_e i^2} = \frac{\rho_{air}}{c}\cdot\frac{\pi}{2}\cdot B^2 r^4 \rho^*_{cop}\rho_{cop}\frac{M_{cop}}{M_{ms}^2} \quad (16)$$

Furthermore, the total moving part mass, M_{ms}, is the sum of the coil mass, M_{cop}, and of the emissive face mass, M_{si}:

$$M_{ms} = M_{cop} + M_{si} \quad (17)$$

Eq. (16) shows that the efficiency is maximal when the masses M_{si} and M_{cop} are equal. It becomes:

$$\eta_{max} = \frac{\rho_{air}}{c}\cdot\frac{\pi}{2}\cdot B^2 r^4 \rho^*_{cop}\rho_{cop}\frac{1}{M_{ms}} \quad (18)$$

This last equation (Eq. (18)) proves the importance of two parameters: the moving part mass, M_{ms}, and the mean value of the radial induction, B, seen by the coil. The efficiency depends on physical parameters of the device and not on the sound level.

6. Structure using one axially polarized ring permanent magnet

6.1. Geometry

The motor has a rather original structure, as its stator is constituted of permanent magnets only [11–14]. So, the absence of iron suppresses all the effects related to this material, such as eddy currents and the reluctance effect, and which are sources of non-linearities [15]. The first considered structure is a motor using only one ring permanent magnet with axial polarization. Such a configuration is shown in Fig. 4. The non-magnetic substrate is represented in orange[1] and the flat moving coil in blue.

6.2. Calculation of the magnetic field created by one axially polarized ring permanent magnet

Another advantage of the ironless structures is the possibility of obtaining analytical formulations for the magnetic field created by the permanent magnets and thus evaluating the magnetic field all over the moving coil displacements. Therefore, the coulombian model of an axially polarized ring permanent magnet was used and the obtained analytical expressions are based on elliptic inte-

[1] For interpretation of color in Figs. 1–4, 6–13, the reader is referred to the web version of this article.

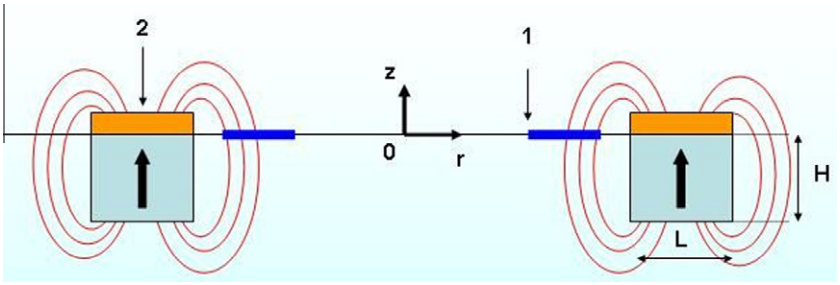

Fig. 4. Motor using one axially polarized ring permanent magnet. Orange: non-magnetic substrate (2), blue: flat moving coil (1).

grals whose numerical evaluation can be carried out quickly with *Mathematica* or *Matlab* [16]. Besides, analytical models are more accurate than numerical ones, especially for structures with small dimensions and allow to carry out easily parametric studies and optimizations.

6.2.1. Methodology

When using the coulombian model of a magnet [17,18] the ring permanent magnet is replaced by two cylindrical planes charged with fictitious magnetic pole surface densities $+\sigma^*$ and $-\sigma^*$. As the polarization of the ring magnet is axial the upper face is charged with the fictitious magnetic pole surface density $+\sigma^* = \vec{J}\cdot\vec{n}$ and the lower face is charged with the fictitious magnetic pole surface density $-\sigma^* = \vec{J}\cdot\vec{n}$, where $\vec{n}$ is the unit vector and $\vec{J}$ is the polarization vector (see Fig. 5). By denoting P a point located on the magnetic charge distribution, the magnetic field $\vec{B}(r,z)$ created by the axially polarized ring permanent magnet in a point M is expressed as follows:

$$\vec{B}(r,z) = \frac{J}{4\pi}\int_{S_{up}} \frac{\overrightarrow{PM}}{\overrightarrow{PM}^3} ds - \frac{J}{4\pi}\int_{S_{low}} \frac{\overrightarrow{PM}}{\overrightarrow{PM}^3} ds$$

where S_{up} is the upper surface area of the ring and S_{low} is the lower surface area. The radial field $B_r(r,z)$ can be obtained by calculating the scalar product between the magnetic field $\vec{B}(r,z)$ and $\vec{u}_r$.

6.2.2. Analytical expression of the radial field $B_r(r,z)$

The radial magnetic field $B_r(r,z)$ created by one axially polarized ring permanent magnet is expressed as follows [19]:

$$B_r(r,z) = -\frac{J}{4\pi}\sum_{n=1}^{2}(-1)^{n-1}\frac{t_n k_n^+}{r}\sqrt{\frac{r_{in}}{r}}\left(K(k_n^+) + \frac{r-r_{in}}{r+r_{in}}\Pi(h^+,k_n^+)\right) + \frac{J}{4\pi}\sum_{n=1}^{2}(-1)^{n-1}\frac{t_n k_n^-}{r}\sqrt{\frac{r_{out}}{r}}\left(K(k_n^-) + \frac{r-r_{out}}{r+r_{out}}\Pi(h^-,k_n^-)\right) \quad (19)$$

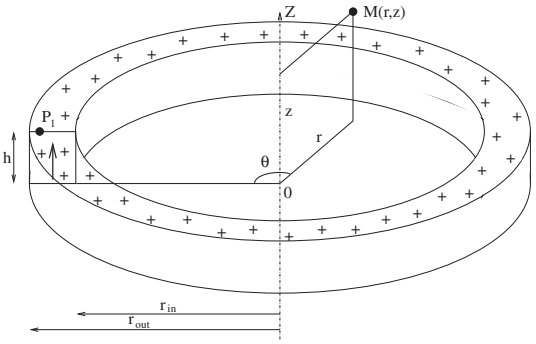

Fig. 5. Ring magnet geometry: inner radius r_{in}, outer radius r_{out}, height $h = z_2 - z_1$; axial polarization.

where r_{in} is the inner radius of the ring permanent magnet, r_{out} is the outer radius, $h = z_2 - z_1$ is the height of the ring. Moreover, the previous relation uses the following parameters:

$$\begin{aligned} k_n^+ &= \frac{4rr_{in}}{(r+r_{in})^2 + t_n^2} \\ k_n^- &= \frac{4rr_{out}}{(r+r_{out})^2 + t_n^2} \\ h^+ &= \frac{4rr_{in}}{(r+r_{in})^2} \\ h^- &= \frac{4rr_{out}}{(r+r_{out})^2} \\ t_1 &= z - z_2 \\ t_2 &= z - z_1 \end{aligned} \quad (20)$$

where $K(k)$, $E(k)$ et $\Pi(h,k)$ are elliptic integrals of the first, second and third kind.

6.2.3. Radial field produced in the air gap

The evolution of the radial field created by an axially polarized ring versus the radial distance r is evaluated for the following values: $h = z_2 - z_1 = 3$ mm, $z_2 = 0$ mm, $r_{in} = 8$ mm, $r_{out} = 11$ mm, $J = 1.4$ T, and represented in Fig. 6. Fig. 6 shows that the radial field decreases as $1/r^2$ when r decreases. So, the Lorentz Force on the coil is high when the latter is close to the ring magnet: the air gap between the ring inner face and the flat moving coil must be as small as possible, once manufacturing and vibration constraints are taken into account.

Calculations of the mean radial field created by an axially polarized ring permanent magnet are carried out for a 7.5 mm outer radius flat moving coil and two air gap values (Fig. 7): 0.5 mm, corresponding to a 8 mm inner radius ring permanent magnet (blue curve) and 1 mm, corresponding to a 8.5 mm one (orange curve). As a result, the mean field value obtained for the 1 mm air gap is at least 40% lower than for the 0.5 mm one and the corresponding

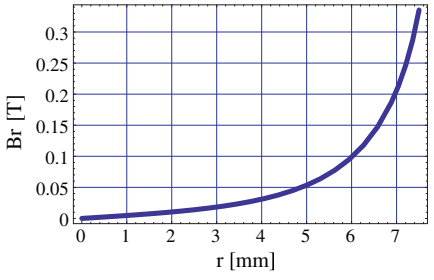

Fig. 6. Calculated radial field created by an axially polarized ring magnet in the air gap versus the radial distance r (mm) for $h = z_2 - z_1 = 3$ mm, $z_2 = 0$ mm, $r_{in} = 8$ mm, $r_{out} = 11$ mm, $J = 1.4$ T.

efficiency would be the half. So, a 8 mm inner radius ring permanent magnet should be used.

6.3. Optimal axial position of the moving coil

For given dimensions of the moving coil and of the ring permanent magnet the axial position of the moving coil can be optimized to reach the highest radial magnetic field mean value in the coil and thus the highest exerted force. The chosen dimensions are 5 mm and 7.5 mm for the coil inner and outer radii, 8 mm and 11 mm for the ring magnet inner and outer radii. The magnet polarization is $J = 1.4$ T.

Moreover, the calculations Fig. 7 are carried out for the coil located at the same axial position as the upper face of the ring magnet, that is at $z = 0$. So, Fig. 7 also shows that $\langle Br \rangle$ would be maximal in the coil if the coil were located 0.2 mm above the magnet upper face. Consequently, a 0.2 mm spacer should be used between the ring magnet upper face and the substrate to locate the coil at this optimal axial position.

6.4. Optimal dimensions of the axially polarized ring permanent magnet

Now, the magnet ring optimal dimensions have to be determined. The aim is to create the highest mean radial magnetic field with the smallest magnet volume possible.

6.4.1. Optimal height of the ring

The radial magnetic field created by a ring permanent magnet of given radii increases when the ring axial height increases (Fig. 8). However, packaging and cost considerations lead to the search for trade-offs. Moreover, the field increase is not linear with the ring magnet height. While a 1 mm height would not create a strong enough field, the increase up to 3 mm would not be economically satisfactory as the volume relative increase becomes greater than the field one. Thus, 2 mm or 2.5 mm seems to be the permanent magnet ring optimal height.

6.4.2. Optimal radial width of the ring

The study of the influence of the magnet width on the mean radial field produced by the axially polarized ring permanent magnet leads to the same conclusions as the ones obtained for the axial height. Fig. 9 shows that there is an interesting trade-off when the radial width reaches 2 mm. Indeed, smaller radial widthes lead to a 40% decrease of the radial field created. On the other hand, greater radial widthes increase the field but the magnet volume becomes too large to be economically acceptable.

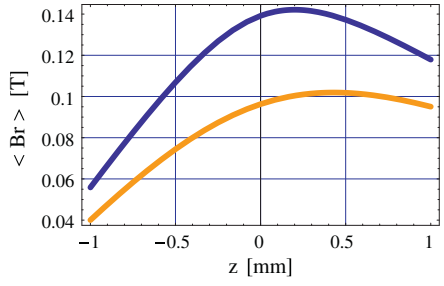

Fig. 7. Calculated mean radial field $\langle Br \rangle$ versus z (mm). Coil outer radius: 7.5 mm. Magnet: $h = z_2 - z_1 = 3$ mm, $z_2 = 0$ mm, $J = 1.4$ T. Blue: 0.5 mm air gap, $r_{in} = 8$ mm, $r_{out} = 11$ mm. Orange: 1 mm air gap, $r_{in} = 8{,}5$ mm, $r_{out} = 11{,}5$ mm.

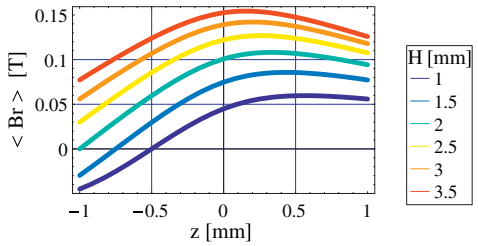

Fig. 8. Calculated mean radial field $\langle Br \rangle$ created by an axially polarized ring magnet versus z (mm) for several ring axial heights, $H = z_2 - z_1$ and $z_2 = 0$ mm, $r_{in} = 8$ mm, $r_{out} = 11$ mm, $J = 1.4$ T.

7. Motor using two axially polarized ring permanent magnets

A motor made of two axially polarized ring permanent magnets in repulsion and separated by a substrate and a spacer is considered now. Such a structure creates a symmetric radial field higher than the disymmetric radial field produced by a motor using only one axially polarized ring permanent magnet. Fig. 10 shows the mean radial field $\langle Br \rangle$ produced by a motor using one axially polarized ring permanent magnet (orange curve) and by a motor constituted of two axially polarized ring permanent magnets in repulsion (blue curve). The total magnet volume is kept constant, so the magnet dimensions are $r_{in} = 8$ mm, $r_{out} = 11$ mm and $h = z_2 - z_1 = 3$ mm, for the single magnet, whereas $h = z_2 - z_1 = 1.5$ mm for each magnet for the two magnet design. Thus, the structure with two magnets creates a mean radial magnetic field 12% higher than the single magnet one. However, the single magnet structure is more easily assembled and thus constitutes a better choice.

8. Motor using two radially polarized ring permanent magnets

Motor structures with radially polarized ring permanent magnets have to be considered, though they are more difficult to manufacture and thus more expensive than axially polarized ones (Fig. 11).

The coulombian model of a magnet is used again to express analytically the radial field produced by this configuration.

8.1. Analytical expression of the radial field created by a radially polarized ring permanent magnet

The radial component of the magnetic field created by a radially polarized ring permanent magnet can be expressed as follows:

$$B_r(r,z) = \frac{J}{4\pi}\sum_{i=1}^{2}\sum_{k=1}^{2}(-1)^{i+k}\left(g(i,k,2\pi) - g(i,k,0)\right) \tag{21}$$

with

$$g(i,k,\tilde{\theta}) = 2(z-z_k)f\left(r^2+(z-z_k)^2, r^2+r_i^2+(z-z_k)^2, rr_i, -r^2-2(z-z_k)^2, \tilde{\theta}\right)$$

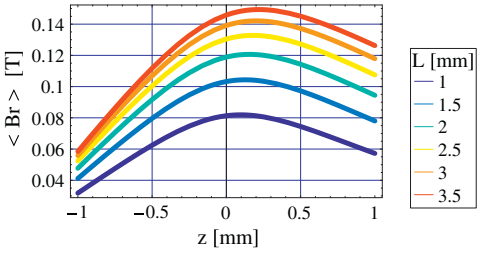

Fig. 9. Calculated mean radial field $\langle Br \rangle$ created by an axially polarized ring magnet versus z (mm) for several ring permanent magnet radial widths $r_{in} = 8$ mm, $r_{out} = 8 + L$ mm, $H = z_2 - z_1 = 3$ mm, $z_2 = 0$ mm, $J = 1.4$ T.

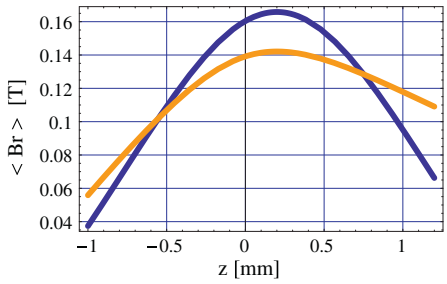

Fig. 10. Calculated mean radial field $\langle Br \rangle$ in two motors with one (orange) $h = z_2 - z_1 = 3$ mm, or two (blue) $h = z_2 - z_1 = 1{,}5$ mm axially polarized rings, $r_{in} = 8$ mm, $r_{out} = 11$ mm, $J = 1.4$ T.

where

$$
\begin{aligned}
f(a,b,e,c,x,\tilde{\theta}) = {} & \eta(2\xi_1(2ce^2+\xi_2))\mathbf{F}^*[\phi_2,\phi_3] + \eta(-e^2(c-x) \\
& \times (bx\sqrt{2}+2\xi_1)) \times \mathbf{\Pi}^*\left[\phi_1^+,\phi_2,\phi_3\right] + \eta(e^2(c \\
& - x)(bx\sqrt{2}-2\xi_1)) \times \mathbf{\Pi}^*\left[\phi_1^-,\phi_2,\phi_3\right] \\
& - 2\eta ax\left(xe^2 - ce^2\sqrt{2} + b\xi_1\right) \\
& \times \mathbf{\Pi}^*\left[\phi_1^+,\phi_2,\phi_3\right] - 2\eta ax(-xe^2 + ce^2\sqrt{2} \\
& + b\xi_1) \times \mathbf{\Pi}^*\left[\phi_1^-,\phi_2,\phi_3\right] \qquad (22)
\end{aligned}
$$

where $\mathbf{F}^*[\mathbf{x},\mathbf{y}]$ and $\mathbf{\Pi}^*[\mathbf{x},\mathbf{y},\mathbf{z}]$ are elliptic integrals of the first, second and third kind. The parameters ξ_1, ξ_2, η are defined as follows:

$$
\begin{aligned}
\xi_1 &= \sqrt{e^2x(x-c)} \\
\xi_2 &= x(b^2-2e^2) \\
\eta &= \frac{i\sqrt{\frac{-e^2\sin(\tilde{\theta})^2}{(b-2e)^2}}\csc(\tilde{\theta})}{2\sqrt{\frac{-1}{b+2e}}x\xi_1(2ce^2+\xi_2)} \\
\phi_1^{+,-} &= \frac{(b+2e)x}{bx \pm \sqrt{2}\sqrt{xe^2(x-c)}} \\
\phi_2 &= i\sinh^{-1}\left(\sqrt{\frac{-1}{b+2e}}\sqrt{b-2e\cos(\tilde{\theta})}\right) \\
\phi_3 &= \frac{b+2e}{b-2e}
\end{aligned}
\qquad (23)
$$

8.2. Comparison of the radial field created by two ring permanent magnets axially or radially polarized

This section compares the radial field created by two radially polarized ring permanent magnets and the one created by two axially polarized ring permanent magnets in repulsion.

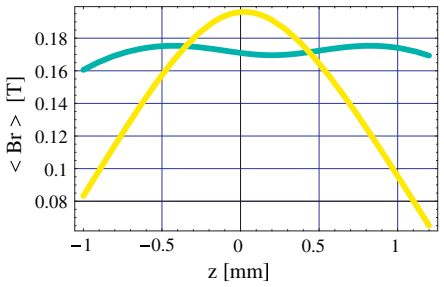

Fig. 12. Calculated mean radial fields produced by two ring permanent magnets radially (blue) or axially (yellow) polarized of same dimensions, $r_{in} = 8$ mm, $r_{out} = 11$ mm, $h = z_2 - z_1 = 2$ mm, $J = 1.4$ T.

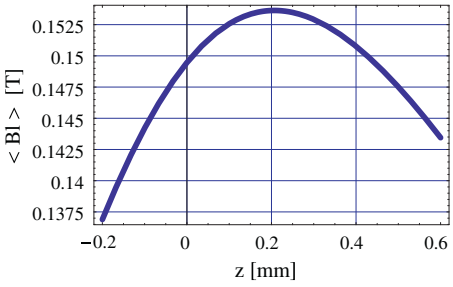

Fig. 13. Calculated force factor mean value $\langle Bl \rangle$ versus coil axial position z.

Fig. 12 shows that two radially polarized ring permanent magnets create a uniform radial field from $z = -1$ mm to $z = +1$ mm, which corresponds to large excursions of the moving coil. However, the mean radial field seen by the moving coil is the same in both structures for z between -0.5 mm and $+0.5$ mm. Consequently, for this restricted clearance, two axially polarized ring permanent magnets seem more interesting than two radially polarized ones.

9. Optimal configuration and Bl values

The optimal configuration resulting from previous studies and discussions is a motor with one axially polarized ring permanent magnet with a 1.4 T polarization, a 8 mm inner radius, a 9 mm outer radius, a $h = 2.5$ mm axial height and a moving coil of 5 mm and 7.5 mm inner and outer radii. The moving coil is supposed to be flat and its length is 1.41 m.

Fig. 13 shows the mean value of the force factor versus the axial position of the moving coil. Thus, the force factor is both high and uniform for z varying from -0.15 mm to $+0.15$ mm, which corresponds to the excursion of the moving coil in our prototype.

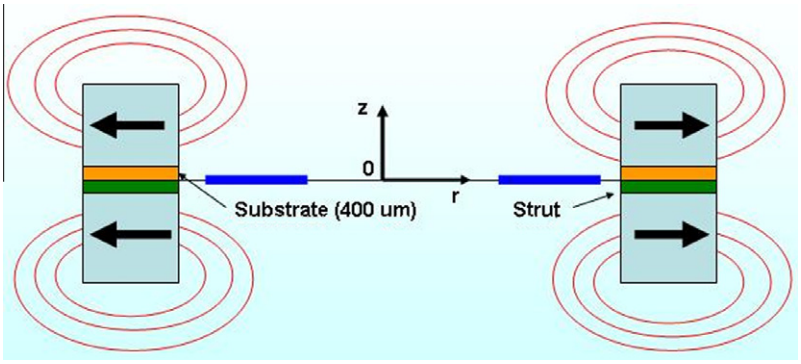

Fig. 11. Motor using two radially polarized ring magnets.

10. Conclusion

This paper presents MEMS electrodynamic loudspeakers dedicated to mobile phone applications.

The purpose is to reach both a high electroacoustic conversion efficiency and a high fidelity acoustic quality. Therefore, a silicon membrane is specially designed and optimized to be rigid and lightweight. Its suspension consist in a set of silicon beams. The moving coil is a planar copper microcoil electroplated on the silicon membrane in a dedicated way. Results are presented for a deep RIE etched 7.5 mm radius silicon membrane structured with 40 stiffening ribs and a 30 μm thick microcoil with 35 turns.

Moreover, the stator of the motor is made with permanent magnets only which are bonded on the substrate. As the iron is source of non-linear effects, its disappearing leads to a far more linear loudspeaker behavior than for classical structures. Besides, these ironless structures are studied and optimized thanks to exact analytical formulations of the magnetic field created by the permanent magnets. Several structures are presented and studied, with either axially or radially polarized ring permanent magnets. They are evaluated and compared with criteria such as the mean radial magnetic field intensity, the magnet volume, the force factor.

Indeed, the acoustic study of the device shows that the efficiency is high when the force factor is high. Moreover, a high transduction quality is achieved when the coil is submitted to a radial magnetic field whose mean value does not vary significantly with the coil displacement.

Eventually, the chosen structure corresponds to a compromise between economics and size and consists in a stator with only one axially polarized ring permanent magnet, which is an interesting trade-off obtained with a relatively small volume of magnet.

Such a MEMS is unique in its function, an electrodynamic loudspeaker, and in its characteristics for an ironless loudspeaker structure: rather thick electroplated copper coil, very rigid silicon emissive surface with large displacements.

References

[1] Lemarquand G. Ironless loudspeakers. IEEE Trans Magn 2007;43(8):3371–4.
[2] Woytasik M, Moulin J, Martincic E, et al. Copper planar microcoils applied to magnetic actuation. Microsystem Technol 2008;14(7):951–6.
[3] Je S, Rivas F, Diaz R, Kwon J, Kim J, Bakkaloglu B, et al. A compact and low-cost mems loudspeaker for digital hearing aids. IEEE Trans Biomed Circ Syst 2009;3(5):348–58.
[4] Cheng MC, Huang WS, Huang SR. A silicon microspeaker for hearing instruments. J Micromech Microeng 2004;14:859–66.
[5] Yi SH, Kim ES. Micromachined piezoelectric microspeaker. Jpn J Appl Phys 2005;44(6A):3836–41.
[6] Rangsten P, Smith L, Rosengren L, Hok B. Electrostatically excited diaphragm driven as a loudspeaker. Sensors Actuators A 1996;52:211–5.
[7] Ko SC, Kim YC, Lee SS, Choi SH, Kim SR. Micromachined piezoelectric membrane acoustic device. Sensors Actuators A 2003;103:130–4.
[8] Shahosseini I, Lefeuvre E, Woytasik M, Moulin J, Leroux X, Edmond S, et al. Towards high fidelity high efficiency mems microspeakers. In: IEEE sensors conference; 2010. p. 2426–30.
[9] Pierce AD. Acoustics, Acoustical Society of America, ISBN 0-88318-612-8; 1989.
[10] Skudrzyk EJ. The foundations of acoustics. Springer-Verlag; 1971.
[11] Merit B, Lemarquand G, Lemarquand V. In pursuit of increasingly linear loudspeaker motors. IEEE Trans Magn 2009;45(6):2867–70.
[12] Ravaud R, Lemarquand G, Lemarquand V, Depollier C. Ironless loudspeakers with ferrofluid seals. Arch Acoust 2008;33(4S):3–10.
[13] Remy M, Lemarquand G, Castagnede B, Guyader G. dsfsda ff. Ironless and leakage free voice-coil motor made of bonded magnets. IEEE Trans Magn 2008;44(11).
[14] Merit B, Lemarquand G, Lemarquand V. Performances and design of ironless loudspeaker motor structures. J Appl Acoust 2010;71(6):546–55.
[15] Ravaud R, Lemarquand G. Modelling an ironless loudspeaker by using three-dimensional analytical approaches. Prog Electromagn Res 2009;91:53–68.
[16] Ravaud R, Lemarquand G. Comparison of the coulombian and amperian current models for calculating the magnetic field produced by arc-shaped permanent magnets radially magnetized. Prog Electromagn Res 2009;95:309–27.
[17] Furlani EP, Knewston M. A three-dimensional field solution for permanent-magnet axial-field motors. IEEE Trans Magn 1997;33(3):2322–5.
[18] Perigo E, Faria R, Motta C. General expressions for the magnetic flux density produced by axially magnetized toroidal permanent magnets. IEEE Trans Magn 2007;43(10):3826–32.
[19] Babic SI, Akyel C. Improvement in the analytical calculation of the magnetic field produced by permanent magnet rings. Prog Electromagn Res C 2008;5:71–82.